Large Spin Diffusion Length in an Amorphous Organic Semiconductor

J. H. Shim,[1] K. V. Raman,[1] Y. J. Park,[1,2] T. S. Santos,[1] G. X. Miao,[1] B. Satpati,[3] and J. S. Moodera[1]

[1]*Francis Bitter Magnet Laboratory, MIT, Cambridge, Massachusetts 02139 USA*

[2]*Nano-device Research Center, Korea Institute of Science and Technology, Seoul, Korea*

[3]*Paul Drude Institute for Solid State Electronics, Berlin, Germany*

(Received 20 February 2008; published 4 June 2008)

We directly measured a spin diffusion length (λ_s) of 13.3 nm in amorphous organic semiconductor (OS) rubrene ($C_{42}H_{28}$) by spin polarized tunneling. In comparison, no spin-conserved transport has been reported in amorphous Si or Ge. Absence of dangling bond defects can explain the spin transport behavior in amorphous OS. Furthermore, when rubrene barriers were grown on a seed layer, the elastic tunneling characteristics were greatly enhanced. Based on our findings, λ_s in single-crystalline rubrene can be expected to reach even millimeters, showing the potential for organic spintronics development.

DOI: 10.1103/PhysRevLett.100.226603 PACS numbers: 72.25.Dc, 72.80.Le, 75.47.−m, 85.75.−d

The emerging field of organic spintronics is merging the two hot fields—organic electronics and spintronics [1]. Chemical tunability of electrical properties in OSs with a bottom-up approach, along with the mechanical flexibility and low-cost fabrication processes [2], has given rise to organic-electronic devices, such as light-emitting diodes (OLED) and field effect transistors (OFET). From the spintronics viewpoint, of growing interest is the potential to transport and manipulate spin information in OSs. Spin-orbit and hyperfine interactions, the main cause of spin-decoherence, being weak in OSs [3], suggest a large λ_S in these materials. However, only a few studies to date explore the spin transport properties in OSs [4–7]. Xiong *et al.* [5] reported spin transport through a thick layer of tris-8-(hydroxyquinoline) aluminum at low temperature in $La_{0.7}Sr_{0.3}MnO_3$/tris-8 -(hydroxyquinoline)aluminium/Co spin valve (SV) structure. We demonstrated spin-conserved tunneling through ultrathin tris-8-(hydroxyquinoline) aluminum barriers at room temperature in magnetic tunnel junctions (MTJs) [6]. Recently, Pramanik *et al.* [7] estimated a long λ_S using a Co/tris-8 -(hydroxyquinoline)aluminium/Ni nanowire SV structure. Here, we carried out spin transport studies through rubrene, and directly measured λ_S using the Meservey-Tedrow spin polarized tunneling (SPT) technique to obtain spin polarization P (the ratio $(n_\uparrow - n_\downarrow)/(n_\uparrow + n_\downarrow)$, where $n_{\uparrow(\downarrow)}$ are spin up (down) tunneling electrons) [8].

Rubrene (5,6,11,12-tetraphenylnaphthacene) is a π-conjugated molecular semiconductor having high charge-carrier mobility ($\sim$20 $cm^2/V\,s$) as seen from OFET studies [9]. The mechanism of charge injection and transport through an OS is yet to be well understood [10]: in the polaronic model, electrical conduction is by hopping through the weakly-coupled, localized molecular levels [11,12]. In our tunneling studies, using various thicknesses of rubrene (down to a few monolayers) as barriers, a large λ_S is observed at low temperature. Although Mott's Variable Range Hopping (VRH) theory [13] seem to fit the transport behavior at high temperatures, we see significant spin-conserved tunneling through rubrene even at room temperature.

Full description of *in situ* thin film junction fabrication is discussed in earlier publications [6,8]. All film layers for the tunnel junctions (area 200 μm $\times$ 200 μm) were thermally evaporated in a high vacuum deposition chamber (base vacuum $\sim 10^{-8}$ torr), onto clean glass substrates using shadow masks. Rubrene (Aldrich, sublimed) barrier films with six different thicknesses (4 nm to 18 nm) were grown in a single run, ensuring the same growth conditions. For SPT junctions, Al/rubrene/Co was used without (rubrene junction) or with (hybrid junction) a $\sim$0.5 nm thick seed layer of Al_2O_3 by a short oxygen plasma exposure of the bottom Al film. MTJs were created by replacing Al with Fe. SPT junctions were cooled to 0.45 K in a ^{3}He cryostat and the conductance vs bias was measured to obtain P. Al was superconducting (SC) below 2.9 K and acted as the spin detector in presence of a magnetic field, applied parallel to the film plane [8].

Figures 1(a)–1(d) show the cross-sectional transmission electron microscope (XTEM) image of junctions grown at either 80 or 295 K for both rubrene and hybrid junctions. Film thickness was monitored *in situ* using a quartz crystal sensor, and the nominal thickness of rubrene was 2.2 nm (assuming a density of 1.35 g/cm^3) for all these XTEM samples. These micrographs show rubrene layers to be amorphous, with complete coverage having smooth and sharp interfaces with metal electrodes (no visible intermixing). It is seen that the actual thickness of rubrene grown at 80 K is twice the nominal value (for both rubrene and hybrid junctions) compared to 295 K growth. This is attributed to a higher sticking coefficient at 80 K, where the van der Waals forces at the substrate surface can be expected to dominate over the thermal energy of the adsorbed OS molecules. Moreover, these images also show that the thickness of the rubrene films nearly doubled when grown on Al_2O_3, than when grown directly onto the metal. This may be due to a different growth mode for the rubrene layer, influenced by the dielectric/OS interface [14].

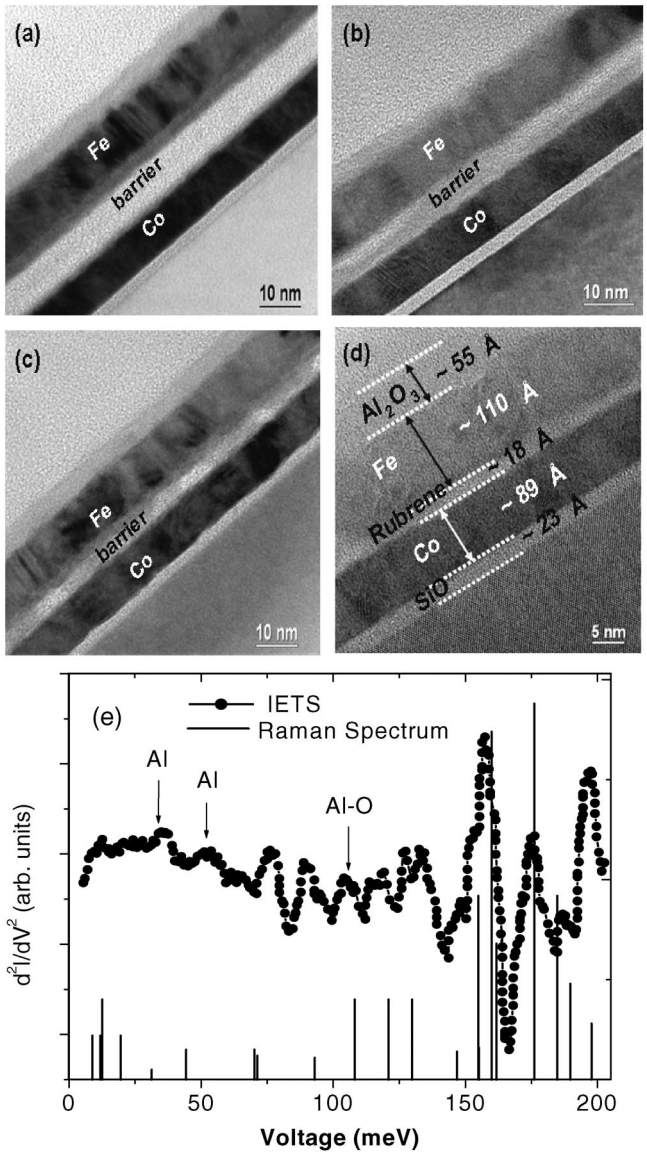

FIG. 1. XTEM images for 8 Co/barrier/10 Fe junctions (thickness in nm) for barriers grown on (100)Si/SiO_2: 0.5Al_2O_3/2.2 rubrene deposited at 80 K (a), 295 K (b), only rubrene deposited at 80 K (c) and 295 K (d). The layers are identified in (d). IETS for a 15 Al/0.5 Al_2O_3/4.4 rubrene/20 Al junctions taken at 4.2 K and the Raman spectrum (lines) for single-crystalline rubrene are shown (e). The peaks due to Al phonon modes and Al-O bond-stretching mode are identified.

Below, we use the film thickness inferred from our XTEM studies.

Inelastic tunneling spectroscopy (IETS), d^2I/dV^2 vs V, was adopted to probe the quality of rubrene barrier [15]. In the IETS data shown in Fig. 1(e), peaks match with the molecular vibrational modes in Raman spectrum for rubrene single crystal, corresponding to the intramolecular interactions [16]. This shows that the rubrene molecules are not chemically altered during our thin film growth.

As expected for tunneling, there was an exponential increase of junction resistance as a function of rubrene thickness. The junctions showed parabolic conductance vs bias dependence, with no zero bias anomalies at any temperature, confirming the sharpness of Co/rubrene interface, without any intermixing (as also seen in XTEM) [6]. At 0.45 K, far below the SC transition of Al, the tunnel conductance vs bias in zero field [Fig. 2(a)] shows negligible conductance at zero bias, confirming the high quality of the tunnel barriers. The observation of a clear SC energy gap in Al shows that the conduction is by tunneling [8]. However, for the rubrene junctions, the shape of the conductance with bias in the SC gap region (slightly faster increase with bias) suggests the existence of inelastic conduction mechanism [17,18]. The smaller SC gap here is due to slightly thicker Al film (not oxidized) [8].

The Zeeman-split asymmetric conductance curve in an applied field allowed us to determine P values of 30% and 10% for electrons tunneling from Co through the rubrene and hybrid barriers, respectively. (Similarly, P_{Co} for Co with Al_2O_3 barrier is 40–42% [19].) This is remarkable since tunneling appears to occur in multiple steps between the localized states in the OS, as will be shown later. The significantly lower value of P for rubrene junctions can be attributed to spin-flip scattering at the M-OS interface, in addition to inelastic hopping that may occur within the barrier. In Fig. 2(b), the determined P values for different thicknesses of rubrene in hybrid junctions show nearly an exponential decay with increasing rubrene thickness, and remarkably, $P > 12\%$ is observed even for a 15 nm thick rubrene barrier. From an exponential fit to the data taking P_{Co} as 42%, λ_S comes out as 13.3($\pm$0.6) nm. This is a

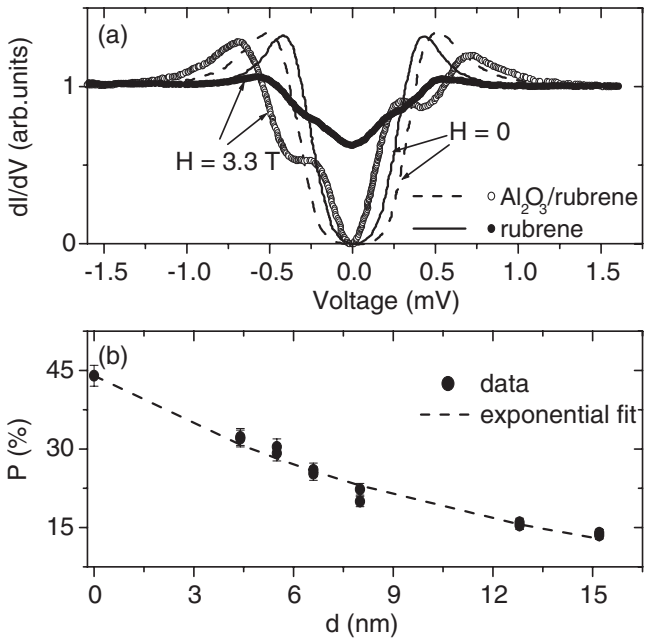

FIG. 2. Tunnel conductance vs bias at 0.45 K with and without an applied magnetic field for two types of junctions: 3.8 Al/barriers/15 Co with 0.5 Al_2O_3/5.5 rubrene or 6.0 rubrene as barriers. (b) Measured P vs rubrene film thickness d, showing the exponential dependence.

direct and clear measurement of λ_S in an OS. At higher temperatures, inelastic transport or hopping through localized molecular and/or trap states in disordered films reduce the mobility and hence can decrease λ_S [1].

In the past, spin transport studies with amorphous Si and Ge tunnel barriers spin polarization was absent [18,20]. But recent reports on single-crystalline Si show $\lambda_S \gg 100\ \mu$m [21,22]. In analogy with Si, our observation of long λ_S in an amorphous OS is noticeably significant. A carrier mobility of $\sim 10^{-6}$ cm^2/V s is reported in amorphous rubrene, whereas in single crystals, the mobility is 7 orders of magnitude higher [23]. Thus, a λ_S of 13.3 nm in amorphous rubrene is highly promising, and one can expect orders of magnitude improvement in crystalline rubrene.

For the SPT junctions, from the current-voltage (I-V) curve, the effective barrier height Φ and thickness d were extracted using the BDR tunneling model [24]. The I-V data at 4.2 K (see Fig. 3 inset) yielded Φ (and d) of 0.45 eV (4 nm) for hybrid and 2.2 eV (2 nm) for rubrene junctions, with an asymmetry $\Delta\Phi \sim 0.2$ eV for the hybrid junctions (which is due to the Al_2O_3 present in this case, creating a trapezoidal barrier [24]). The barrier parameters were temperature independent. Insertion of Al_2O_3 seed layer decreased Φ due to the interfacial dipolar modifications [6,25], whereas the deviation of d from the actual thickness suggests that inelastic processes (more for rubrene junctions) contribute significantly to the conduction process [18]. This is seen as well in the steeper conductance increase with bias in the SC energy gap region of Al [see Fig. 2(a)].

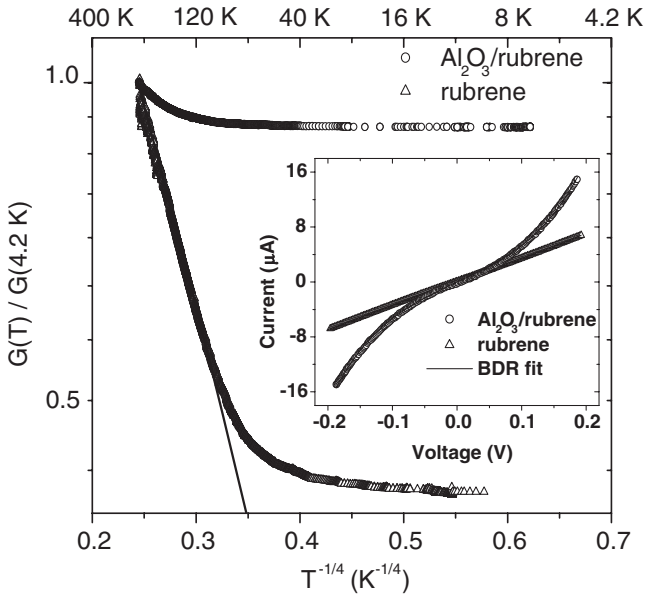

FIG. 3. Temperature dependence of tunnel Conductance for 3.8 Al/6 rubrene/15 Co and 3.8 Al/0.5 Al_2O_3/5.5 rubrene/15 Co junctions. Mott's VRH theory fit (line) to the data at higher temperatures for rubrene-only barrier is shown. Inset shows junction I-V curves at 4.2 K and the fit.

The observation of lower P value (significantly lower for rubrene junctions) is not unexpected since in these amorphous barriers, a higher defect concentration at the M/OS interfaces can be expected [12]. There may be several types of defects at the interface and in the OS. Any mechanism that adds or removes the p_z electron from contributing to the π system gives rise to energy states within the energy gap, leading to defect formation such as a C-H_2 by adding H to the C-H bond, an O_H defect by replacing H with O, or a dangling bond defect ($C_{42}H_{27}$) formed by loosing a H atom [26]. In amorphous Si or Ge, a large number of the dangling bonds ($\sim 10^{19}$ cm^{-3}) exist with their unpaired electron [27], which can be a strong source of spin scattering, as seen experimentally [18,20]. However, in OS, the formation energy for dangling bonds is much higher compared to the other defects mentioned above and hence less dangling bond defects are expected [26]. This can explain our observation of moderately spin-conserved transport in amorphous rubrene.

Transport behavior can be dominated by hopping process for barriers containing localized molecular states and/or structural defects. The low bias junction conductance (G) measured as a function of temperature is shown in Fig. 3. G for the rubrene junctions decreased dramatically from 295 to 4.2 K, compared to a small decrease for the hybrid junctions. Mott's VRH model was adopted to satisfactorily explain our G vs T data [18,20,28]. This model predicts that ℓ_{VRH}, the variable range hopping length, increases with decreasing temperature as $T^{-1/4}$ for 3-dimensional case. G, proportional to the probability of such a hop, is given by: $G_{\mathrm{VRH}} \propto \exp(-2\alpha\ell_{\mathrm{VRH}}) = G_0 \exp[-(T^*/T)^{1/4}]$ [13]. For constant density of localized states within a barrier, the parameter T^* scales with α (where α^{-1} is the localization length, ℓ_{loc}) and is calculated from the slope of conductance versus $T^{-1/4}$ plot at higher temperatures. For similar rubrene thickness, obtained value of T^* was $\sim$4500 K for rubrene junction compared to $\sim$15 K for the hybrid junction; in the latter case, the fitting was only for a small temperature range. This implies that the electronic states contributing to conduction in OS have different ℓ_{loc}, consistent with different growth modes for rubrene and hybrid junctions. Inelastic tunneling (via hopping) can occur when the barrier thickness is greater than ℓ_{loc}. Thus for hybrid junctions, ℓ_{loc} is large with conduction occurring mostly by elastic and resonant tunneling, resulting only in a marginal increase of G with T. On the other hand, for the rubrene junctions having a smaller ℓ_{loc}, the conduction appears to occur via inelastic hopping through localized states, resulting in a stronger $G(T)$ dependence. Thus, with increase in rubrene film thickness, especially in a disordered layer, the probability of direct tunneling diminishes, and the conduction is dominated by inelastic transport in a wider temperature range.

The above results show that having Al_2O_3 seed layer greatly enhances the spin transport in the OS. As a further confirmation, we performed tunnel magnetoresistance

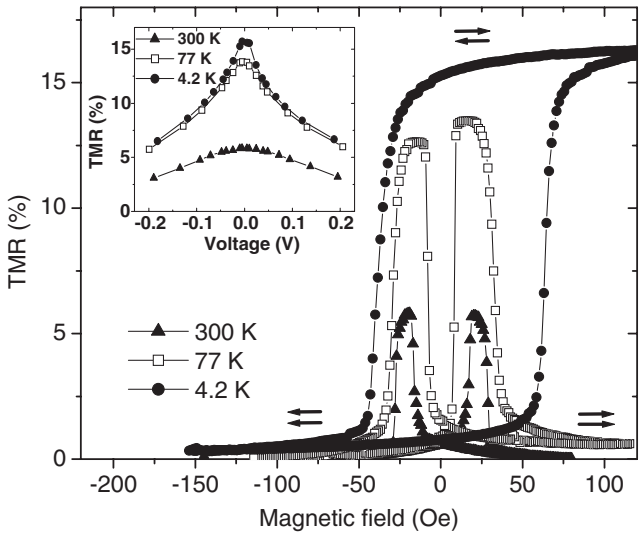

FIG. 4. Resistance variation with applied magnetic fields for the MTJ structure 8 Co/0.5 Al_2O_3/4.6 Rubrene/10 Fe/1.5 CoO junction showing TMR. The data at 4.2 K shows the exchange bias due to the antiferromagnetic CoO over Fe. The lines through the data points are guides to the eye. The inset shows the bias dependence of TMR. The arrows indicate the magnetic configuration of Co and Fe electrodes at various applied fields.

(TMR) measurements in hybrid barrier MTJs: TMR is defined as $\Delta R/R = (R_{AP}\text{-}R_P)/R_P$, where R_{AP} and R_P are the junction resistances for antiparallel and parallel magnetization of the Co and Fe, respectively [29,30]. Julliere's model predicts a large TMR in an MTJ as a result of spin-conserved tunneling [8,29]. Figure 4 shows the TMR for an MTJ measured at 10 mV, with values of 6, 13, and 16% at 295, 80 and 4.2 K, respectively. In contrast, no TMR was observed in rubrene junctions. The decrease in TMR with increasing temperature is common in MTJs and is discussed in the literature, whereas a stronger temperature dependence can be expected due to the larger defect density in the barrier [31]. In addition, as mentioned earlier, at higher temperatures, inelastic transport in these disordered films would decrease λ_S, leading to a lower TMR. The slow decrease of TMR with applied voltage (shown in Fig. 4 inset) and the parabolic conductance vs bias behavior, with no zero bias anomalies, support the MTJs are of high quality [19].

In summary, our studies of spin tunneling and transport in junctions with rubrene barriers show a long λ_S, despite the amorphous nature of the OS barriers. Rubrene barriers with an Al_2O_3 seed layer enhanced the spin transport and attributed to improved growth of OS. These observations can be expected to provide a platform for future investigations as well as the development of OS based spin devices with rubrene or other high mobility organic compounds.

This work was funded by the KIST-MIT program and the ONR grant.

[1] W. J. M. Naber, S. Faez, and W. G. van der Wiel, J. Phys. D **40**, R205 (2007).
[2] J. A. Rogers, Science **291**, 1502 (2001).
[3] S. Sanvito and A. R. Rocha, Journal of Computational and Theoretical Nanoscience **3**, 624 (2006).
[4] L. E. Hueso *et al.*, Adv. Mater. **19**, 2639 (2007).
[5] Z. H. Xiong, D. Wu, Z. V. Vardeny, and J. Shi, Nature (London) **427**, 821 (2004).
[6] T. S. Santos *et al.*, Phys. Rev. Lett. **98**, 016601 (2007).
[7] S. Pramanik *et al.*, Nature Nanotechnology **2**, 216 (2007).
[8] R. Meservey and P. M. Tedrow, Phys. Rep. **238**, 173 (1994).
[9] V. Podzorov *et al.*, Phys. Rev. Lett. **93**, 086602 (2004).
[10] M. A. Baldo and S. R. Forrest, Phys. Rev. B **64**, 085201 (2001).
[11] E. A. Silinsh and V. Capek, *Organic Molecular Crystals: Interaction, Localization, and Transport Phenomena* (AIP Press, New York, 1994).
[12] Z. Bao and J. Locklin, *Organic Field-Effect Transistors* (CRC Press, , Boca Raton, Florida, 2007).
[13] N. F. Mott, Philos. Mag. **19**, 835 (1969).
[14] G. Witte and C. Wöll, Phase Transit. **76**, 291 (2003); Q. Chen, A. J. McDowell, and N. V. Richardson, Langmuir **19**, 10164 (2003).
[15] J. Lambe and R. C. Jaklevic, Phys. Rev. **165**, 821 (1968).
[16] J. R. Weinberg-Wolf, L. E. McNeil, S. Liu, and C. Kloc, J. Phys. Condens. Matter **19**, 276204 (2007).
[17] R. C. Dynes, V. Narayanamurti, and J. P. Garno, Phys. Rev. Lett. **41**, 1509 (1978).
[18] R. Meservey, P. M. Tedrow, and J. S. Brooks, J. Appl. Phys. **53**, 1563 (1982).
[19] J. S. Moodera and G. Mathon, J. Magn. Magn. Mater. **200**, 248 (1999).
[20] G. A. Gibson and R. Meservey, J. Appl. Phys. **58**, 1584 (1985).
[21] B. Huang, D. J. Monsma, and I. Appelbaum, Phys. Rev. Lett. **99**, 177209 (2007).
[22] B. T. Jonker *et al.*, Nature Phys. **3**, 542 (2007).
[23] S. Seo, B. N. Park, and P. G. Evans, Appl. Phys. Lett. **88**, 232114 (2006).
[24] W. F. Brinkman, R. C. Dynes, and J. M. Rowell, J. Appl. Phys. **41**, 1915 (1970).
[25] H. Ishii, K. Sugiyama, E. Ito, and K. Seki, Adv. Mater. **11**, 605 (1999).
[26] J. E. Northrup and M. L. Chabinyc, Phys. Rev. B **68**, 041202(R) (2003).
[27] R. A. Streetand and N. F. Mott, Phys. Rev. Lett. **35**, 1293 (1975).
[28] Y. Xu, D. Ephron, and M. R. Beasley, Phys. Rev. B **52**, 2843 (1995).
[29] M. Julliere, Phys. Lett. A **54**, 225 (1975).
[30] J. S. Moodera, L. R. Kinder, T. M. Wong, and R. Meservey, Phys. Rev. Lett. **74**, 3273 (1995).
[31] J. S. Moodera and R. H. Meservey, *Magnetoelectronics*, edited by Mark Johnson (Elsevier Academic Press, New York, 2004), Ch. 3.